scientific reports

Check for updates

OPEN

Green synthesis, characterization, and photocatalytic activity of superparamagnetic $MgFe_2O_4$@$ZnAl_2O_4$ nanocomposites

Saeid Taghavi Fardood[1]✉, Sara Ganjkhanlu[2], Farzaneh Moradnia[2] & Ali Ramazani[2]

$MgFe_2O_4$@$ZnAl_2O_4$ magnetic nanocomposites were synthesized with the easy and green sol–gel method, and their photocatalytic efficiency was followed toward degradation of reactive blue 222 (RB222) dye under visible light irradiation. Prepared nanocomposites were fully characterized. The SEM and TEM images revealed the spherical morphology of the produced nanocomposites, with average size of 20–25 nm. The XRD pattern of sample exhibited the successful synthesis of the $MgFe_2O_4$@$ZnAl_2O_4$ MNCs with crystallite size 13 nm. The saturation magnetization (Ms) of the nanocomposites was examined using VSM, indicating a value of 6.59 emu/g. The absence of Hc and Mr values confirms the superparamagnetic nature of the nanoparticles. In addition, the surface area was calculated to be 78.109 m^2/g utilizing BET analysis, and the band gap was determined to be 1.88 eV by DRS analysis. The photocatalytic, photolysis, and adsorption performance were investigated and result shown photodegradation activity was higher than others. These results confirm the synergetic effect between the $MgFe_2O_4$@$ZnAl_2O_4$ MNCs and visible light irradiation to degradation of organic dye. The results indicate that rapid degradation of 96% of RB222 dye occurred in just 10 min, with a TOC removal rate of approximately 59%. Furthermore, radical scavenger agents also clarified photodegradation of RB222 dye.

Keywords Photocatalysis, Superparamagnetic nanocomposite, Zinc aluminate, Sol–gel method, Reactive blue 222, Dye degradation

Synthetic dyes are of the chemical compounds that have been consumed in different industries such as leather, pharmaceutical, textile, and paper[1–5]. Because of wide applications and large-scale production of these dyes, they are main part of industrial wastewaters[6–11]. Also, they have high toxicity and chemical stability to degradation by general treatment procedures[12–15]. Thus, common treatment manners are not effective for degradation of organic dyes in wastewater[16,17]. Lately, researchers have been focused to the photocatalysis as the effective and useful method for wastewater treatment owing to their simple operation and high efficiency[18–25].

Utilization of magnetic nanocomposites (MNCs) is one of the useful method to dyes degradation in water and wastewater because they have some merits such as easy and fast separation by constant magnet, economic viability, and recoverability and reusability for several runs[26–32]. Various methods have been reported for preparation the magnetic nanocomposites[33,34]. Sol–gel method by using natural gel is the easy, green, cost-effective, non-toxic, and eco-friendly manner for synthesis the nanocomposites[35–41].

Scientists have demonstrated an increasing interest with the production of magnetic nanoparticles using environmentally friendly synthesis methods. Minghui Li group conducted a study on the synthesis of $MgFe_2O_4$–ZnO heterojunction photocatalysts and examined their effectiveness in degrading Rhodamine B (RhB) dye[42]. In 2022, Makofane et al. reported the green synthesis of $NiFe_2O_4$ nanoparticles using plant extracts from Monsonia burkeana. The nanoparticles were synthesized in cubic spinel crystalline structures. The researchers also investigated how different calcination temperatures affected the photocatalytic activity of the nanoparticles[43]. In 2019, Jia et al. synthesized a Z-scheme $MgFe_2O_4$/Bi_2MoO_6 heterojunction photocatalyst using hydrothermal

[1]Department of Chemistry, Faculty of Science, Ilam University, Ilam 69315-516, Iran. [2]Department of Chemistry, University of Zanjan, Zanjan 45371-38791, Iran. ✉email: s.taghavi@ilam.ac.ir; saeidt64@gmail.com

and ball-milling techniques. They then studied the photocatalytic activity of this catalyst for the removal of malachite green[44].

The research work aimed to synthesis $MgFe_2O_4$@$ZnAl_2O_4$ MNCs using the green sol–gel method. The synthesized materials were subjected to comprehensive characterization employing various techniques, including XRD, TEM, FESEM, BET, DRS, VSM, EDX, and elemental mapping techniques. The research aimed to evaluate the photocatalytic efficacy of magnetic nanocomposites in degrading RB222 dye under visible light irradiation. To find out the optimized conditions, the influence of photocatalyst amount, initial dye concentration, irradiation time, exposure to both dark and visible light, and the reusability of the photocatalyst was investigated. The degrading performance of the dye was verified by the utilization of UV–Vis spectroscopy and total organic carbon (TOC) measurement. Figure 1 depicts the molecular configuration of the RB222 dye.

Experimental

Materials

The TG obtained as a natural gel, was sourced from a bio shop. $Fe(NO_3)_3{\cdot}9H_2O$, $Zn(NO_3)_2{\cdot}6H_2O$, $Al(NO_3)_3{\cdot}9H_2O$, and $Mg(NO_3)_2{\cdot}6H_2O$, as the metal salts, were prepared from Dae-Jung and Merck company.

Characterization of $MgFe_2O_4$@$ZnAl_2O_4$ MNCs

The sample's X-ray diffraction pattern was obtained using an X'Pert-PRO advance X-Ray diffractometer with Cu Kα radiation. Magnetization was assessed using the Meghnatis Kavir Kashan apparatus, and optical properties were recorded through UV–Vis diffuse reflectance spectra with a Shimadzu UV-2550 instrument. The band gap (Eg) was calculated employing Tauc's theory[45]. The TEM image was recorded by using an EM 208S, and SEM (equipped with EDX and Mapping) were obtained with Tescan Mira3. Total organic carbon (TOC) analysis was investigated with Shimadzu TOC-5000, and Jena-Specord 205 spectrophotometer was used for recorded the UV–Vis absorption spectra of dyed solutions. Also, The Belsorp Mini II instrument was utilized to conduct BET analysis.

Synthesis of $MgFe_2O_4$@$ZnAl_2O_4$ MNCs

Taghavi fardood's method was used for synthesis the magnesium ferrite nanoparticles ($MgFe_2O_4$)[46]. 0.2 g of tragacanth gum was added to 40 ml deionized water under magnetic stirring to obtain the transparent gel solution (70 °C for 1 h). In next step, 0.1 g of prepared $MgFe_2O_4$ NPs was added to TG solution and dispersed in it for 2 min under ultrasonic irradiation. Then, 1 mmol $Zn(NO_3)_3{\cdot}6H_2O$, and 2 mmol of $Al(NO_3)_3{\cdot}9H_2O$ were added to the prior solution and dispersed for 2 min. After that, the final solution was stirred for 12 h at 70 °C to achieve dried resin. Obtained resin calcined for 4 h at 600 °C for synthesis $MgFe_2O_4$@$ZnAl_2O_4$ MNCs.

Photocatalytic dye degradation

Photocatalytic experiments were performed utilizing a batch-style photoreaction setup with a 90 W lamp ($\lambda > 400$ nm), and the light intensity was measured using a Lux meter. The intensity of sunlight was examined by a Lux meter. Degradation efficiency was investigated in 50 mL of dye solution by changing amount of $MgFe_2O_4$@$ZnAl_2O_4$ MNCs, initial dye concentration, and irradiation time. When optimum conditions were determined, dye degradation experiment was done in the presence and absence of visible light to confirm the synergistic effect between visible light and synthesized nanocomposites. The efficiency of RB222 dye degradation was computed through UV–Vis spectroscopy at the $\lambda_{max} = 611$ nm. The following equation was used for evaluation the degradation efficiency. A_0 and A are the initial and final absorbance of dye solution, respectively.

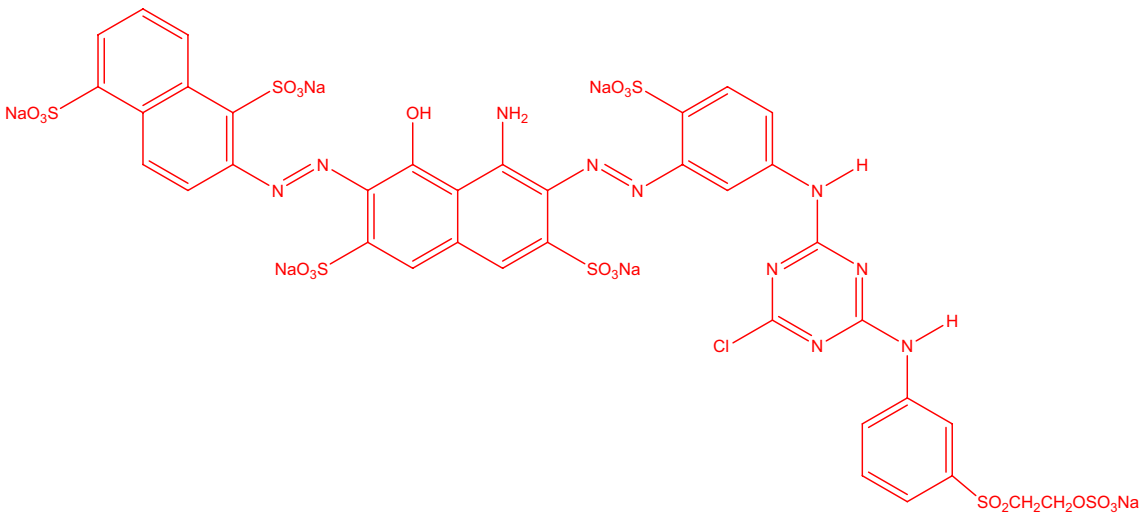

Figure 1. Chemical structure of RB222 dye.

$$\%Degradation = \frac{A_0 - A}{A_0}$$

Result and discussion

Characterization of $MgFe_2O_4$@$ZnAl_2O_4$ MNCs

X-ray diffraction (XRD), and EDX analysis were performed to verify the phase identification, crystallinity, and presence of impurity in synthesized $MgFe_2O_4$@$ZnAl_2O_4$ MNCs. Figure 2 displayed the XRD patterns of the sample. It is evident that all of the diffraction peaks correspond to the cubic spinel phase for $MgFe_2O_4$ (JCPDS card no. 89-4924) and $ZnAl_2O_4$ (JCPDS card no. 73-1961). The estimation of the crystallite size of the sample was conducted using the Scherrer formula[47] and obtained 13 nm. The XRD pattern, devoid of impurities, confirms the successful synthesis of $MgFe_2O_4$@$ZnAl_2O_4$ MNCs through the green sol–gel method.

EDX, and elemental mapping of nanocomposite confirm that sample are contain Mg, Fe, Zn, Al, and O elements with good spatial distribution (Figs. 3, 4).

As can be observe in FESEM and TEM image, magnetic nanocomposites are quite regular in shape and size. Moreover, the TEM image certified the synthesis of $MgFe_2O_4$@$ZnAl_2O_4$ MNCs with a uniform size of nearly 20–25 nm (Fig. 5a,b).

The UV–Vis–DRS spectra of the sample are given in Fig. 6. It can be seen that the bandgap of $MgFe_2O_4$@$ZnAl_2O_4$ MNCs is about 1.88 eV. It is apparent synthesized samples exhibit considerable photocatalytic activity when exposed to visible light irradiation.

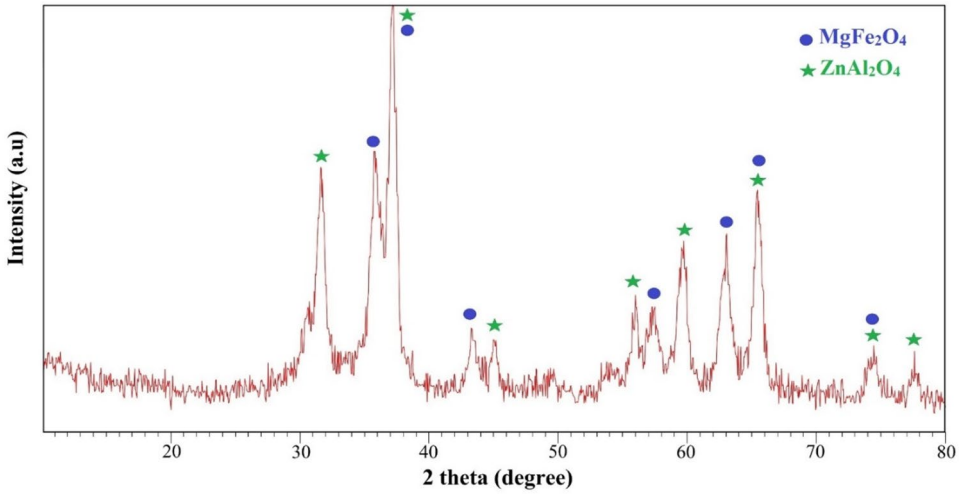

Figure 2. XRD pattern of the $MgFe_2O_4$@$ZnAl_2O_4$ MNCs.

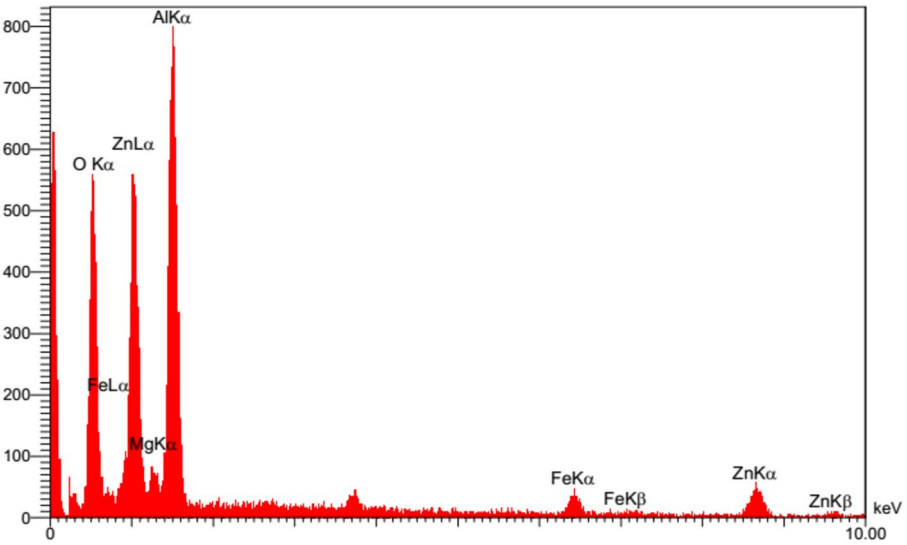

Figure 3. EDX pattern of $MgFe_2O_4$@$ZnAl_2O_4$ MNCs.

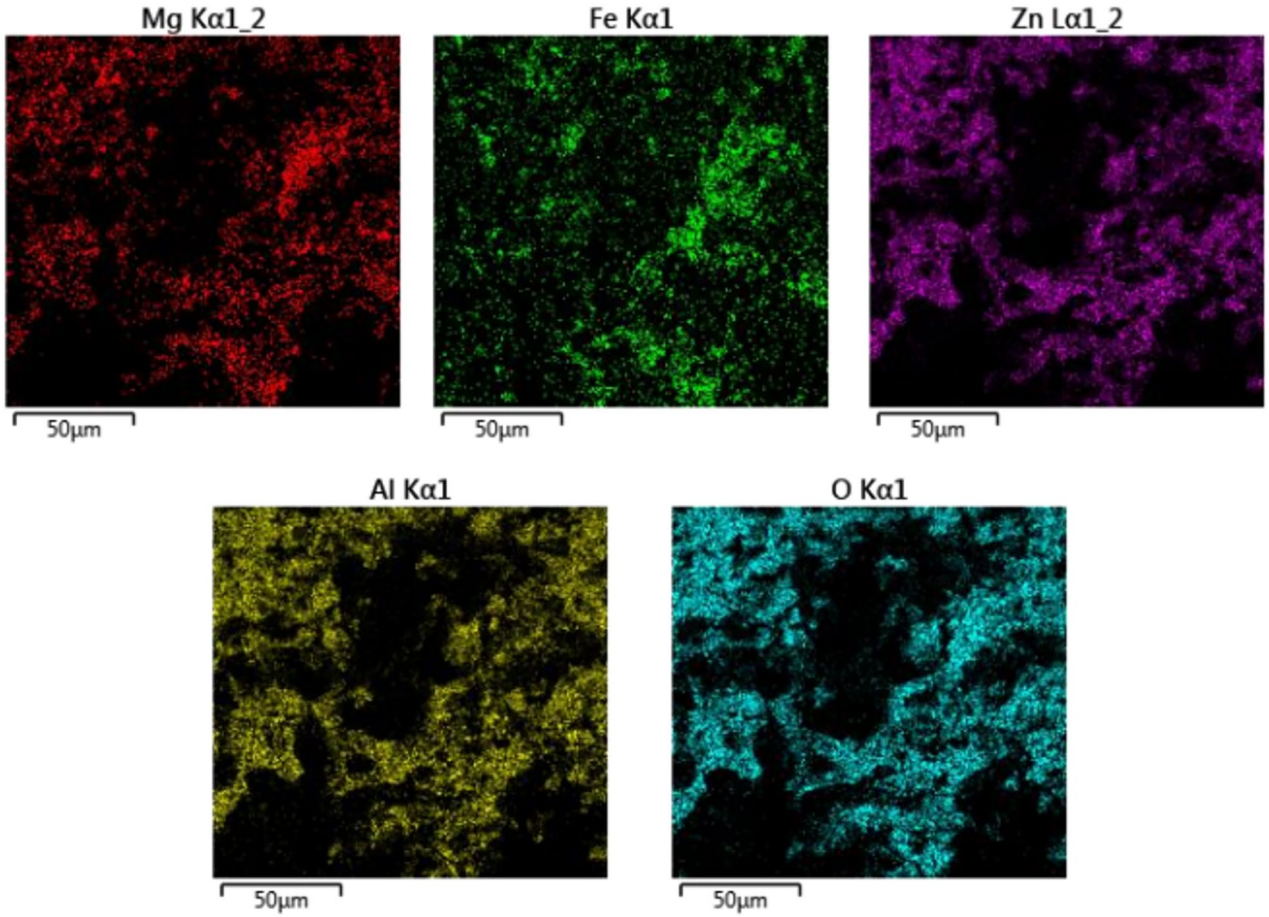

Figure 4. Element mapping images of $MgFe_2O_4$@$ZnAl_2O_4$ MNCs.

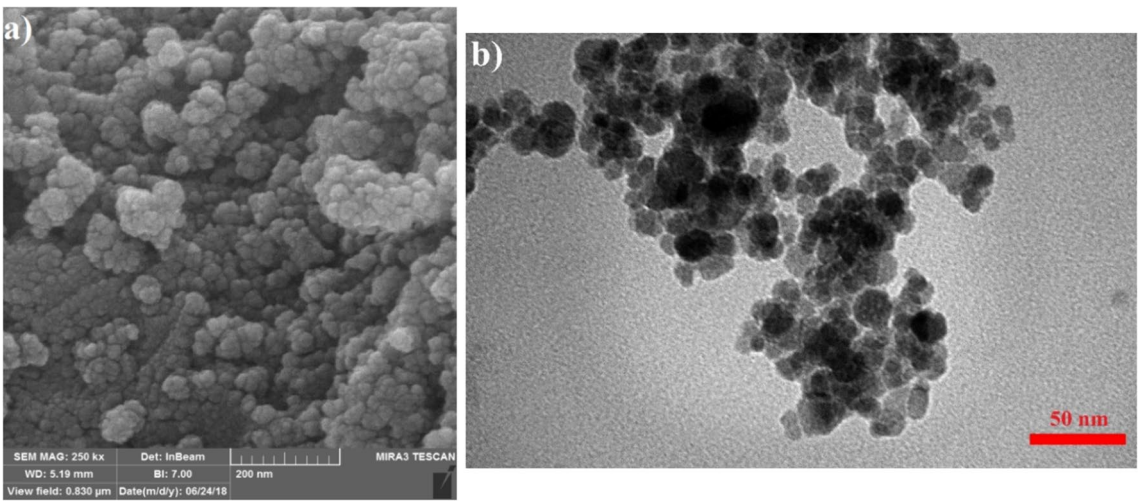

Figure 5. (**a**) FESEM image and (**b**) TEM image of $MgFe_2O_4$@$ZnAl_2O_4$ MNCs.

The magnetic nanocomposite active surface area was appraised with BET analysis. Based to the results, the specific surface area, pore diameter, and total pore volume of sample are 78.109 m^2/g, 14.728 nm, and 0.2876 cm^3/g, respectively. The isotherm for nitrogen adsorption–desorption, as depicted in Fig. 7, verifies the characteristic Type IV behavior with hysteresis loops of Type H1, in accordance with the IUPAC categorization of materials[48].

To study the magnetic properties of synthesized $MgFe_2O_4$@$ZnAl_2O_4$ MNCs, sample was characterized with the VSM technique. According to the magnetic hysteresis (Fig. 8), Ms = 6.59 emu/g and Hc and Mr have equal

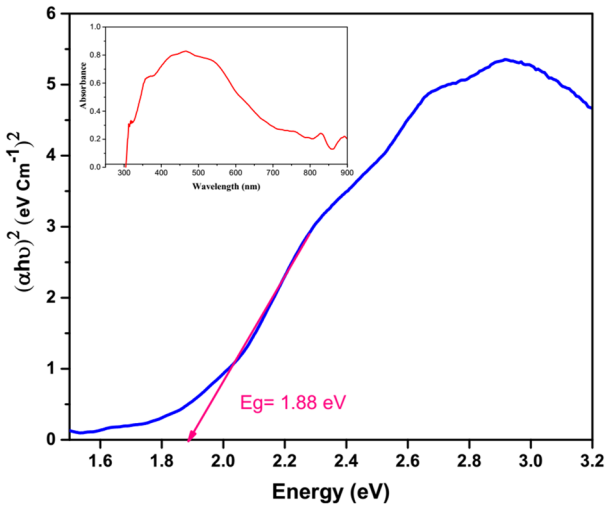

Figure 6. UV–Vis spectrum and Tauc plot of $MgFe_2O_4$@$ZnAl_2O_4$ MNCs.

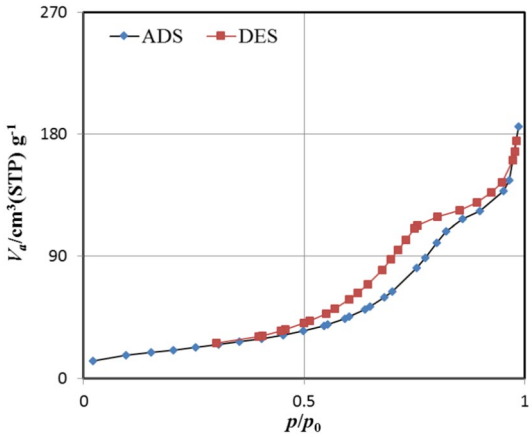

Figure 7. The N_2 absorption/desorption isotherm of the $MgFe_2O_4$@$ZnAl_2O_4$ MNCs.

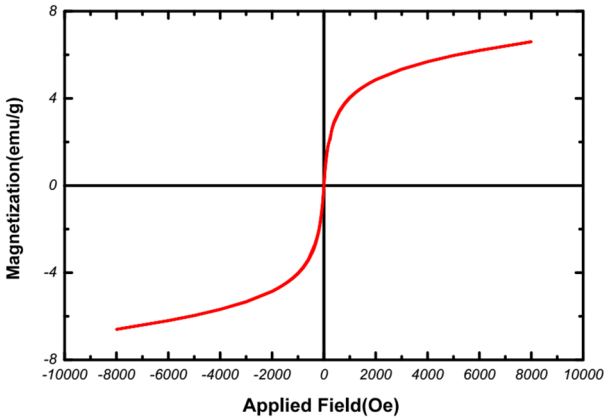

Figure 8. Magnetic hysteresis loop of $MgFe_2O_4$@$ZnAl_2O_4$ MNCs.

values (Hc = Mr = 0) and nanocomposites have superparamagnetic feature and well magnetic feature in the adjacency of a magnet. The $MgFe_2O_4$ MNPs demonstrate a saturation magnetization (Ms) of 13.32 emu/g[49]. Despite a decrease in saturation magnetization, the synthesized nanocomposite retains significant magnetic properties, facilitating easy separation using a magnet. This reduction in Ms confirms the coating of $ZnAl_2O_4$ on $MgFe_2O_4$, as noted in the literature[44,50]. In another study, Taghavi Fardood et al. reported on the green synthesis of $MgFe_2O_4$@CeO_2 nanocomposites and compared their saturation magnetization to $MgFe_2O_4$ NPs. The saturation magnetization (Ms) of $MgFe_2O_4$@CeO_2 MNCs was found to be 3.58 emu/g, representing a significant reduction compared to the $MgFe_2O_4$ sample[49].

Photocatalytic efficiency of $MgFe_2O_4$@$ZnAl_2O_4$ MNCs in degradation of RB222 dye

The photocatalytic activity of $MgFe_2O_4$@$ZnAl_2O_4$ MNCs was investigated by survey the degradation of RB222 dye in ambient condition and natural pH. Photocatalyst experiments was followed by changing different parameters to find the optimum condition and results are given in details. In order to survey the impact of catalyst amount on degradation performance, 0.01–0.025 g of catalyst for RB222 solution was examined. By using 0.02 g of sample, 96% of RB222 dye was removed in 10 min when the initial concentration of dye was 20 mg/l (Fig. 9a). The efficiency of degradation increased when the amount of catalyst was increased from 0.01 to 0.025 g. This could be due to increased production of hydroxyl radicals[51]. Subsequent experiments were carried out by using 0.02 g of nanocomposites as the best amount.

Pollution concentration is one of the important factors that effected the efficiency in photodegradation experiments[49,52]. Hence, degradation of RB222 dye was considered in different concentration (10–40 mg/l of RB222) and constant dosage of $MgFe_2O_4$@$ZnAl_2O_4$ MNCs (0.02 g). Figure 9b, exhibits the variation in degradation efficiency by increasing the concentration. Reduce in degradation performance with increasing concentration can be attributed to the further number of dye molecules whereas photocatalysis (as oxidant agent) dosage is constant. Also, dye molecules functioned as the barrier in solution to attain the light to the surface of photocatalyst and decrease the degradation efficiency[53].

Photocatalytic activity of $MgFe_2O_4$@$ZnAl_2O_4$ MNCs for degradation of RB222 dye was considered with monitoring the performance in three states; photolysis (visible light irradiation without $MgFe_2O_4$@$ZnAl_2O_4$ MNCs), adsorption (magnetic nanocomposites under dark), and photocatalysis ($MgFe_2O_4$@$ZnAl_2O_4$ MNCs under visible light irradiation). In the photolysis state, we don't have degradation for selected dye. In adsorption condition, we have dye removal of 18% for RB222 dye. As shown in Fig. 9c, in photocatalysis state 96% of RB222 dye were degraded at 10 min.

To find the best time of dye degradation, the experiment was followed by using the optimum dosage of catalyst and dye concentration at different irradiation time, and their results are given in Fig. 9d. The lambda max of RB222 is located at 611 nm, and it is clear that degradation performance is certified by a decrease in absorbance maximum values when irradiation time increased. It is noticeable that 96% of RB222 were degraded in 10 min.

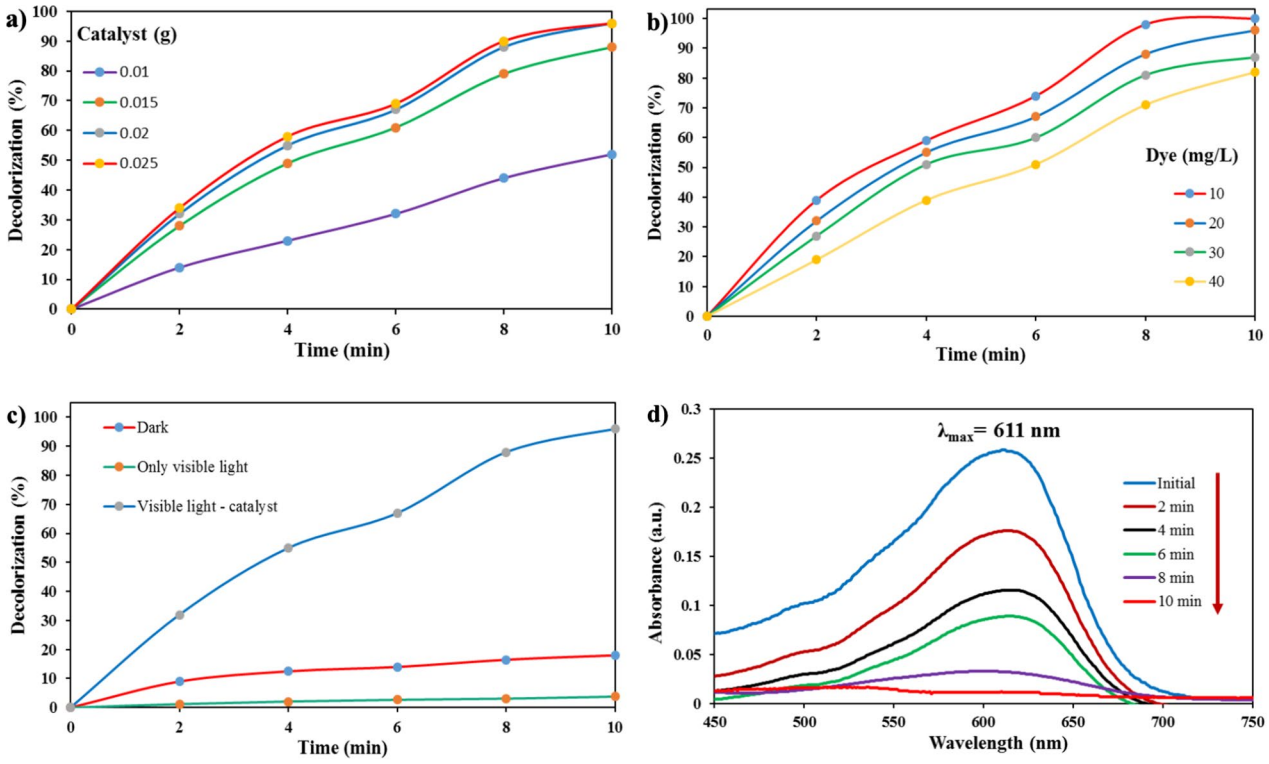

Figure 9. The effect of (**a**) photocatalyst dosage, (**b**) the initial dye concentration, (**c**) light irradiation and (**d**) time on the removal of RB222 dye (%) at room temperature.

Additionally, the removal of TOC from the RB222 dye was evaluated both before and after the degradation test under identical conditions. The findings revealed a 59% reduction in the TOC content of the RB222 dye. This unique efficiency in short time confirm that synthesized nanocomposites are useful photocatalysis in ambient conditions and visible-light region for degradation of RB222 dye.

In photocatalytic reactions, crucial species influencing activity include singlet oxygen ($^1O_2$), hydroxy free radicals ($^{\cdot}OH$), and superoxide radicals ($O_2^{\cdot-}$)[54–56]. Radical scavenging studies using KI, NaN_3, and p-benzoquinone (BQ) were conducted to elucidate the involved reactive species, as depicted in Fig. 10. In the absence of scavengers, RB222 dye removal in 10 min reached 96%. However, with KI and NaN_3, removal decreased to 47% and 36% respectively. Conversely, BQ had minimal impact on the selected dye. These results highlight the significant roles of $^1O_2$ and $OH^{\cdot}$ in the photocatalytic degradation of $MgFe_2O_4$@$ZnAl_2O_4$ MNCs. NaN_3 exhibited superior efficacy over KI, while BQ had a negligible effect on RB222 dye degradation. Thus, photodegradation predominantly occurs via hydroxyl radical and singlet oxygen mechanisms.

In order to survey the stability and recyclability features of the $MgFe_2O_4$@$ZnAl_2O_4$ MNCs, cyclic experiments were performed. The photocatalytic experiments were executed in optimized condition under visible light. Then, magnetic nanocomposites were separated by using the external magnet and washed with deionized water, and next run was carried out with the fresh dye solution. As shown in Fig. 11, the photocatalytic efficiency of the sample reduced slightly after five cycles. However, the degradation performance was remaining up to 96% and 92% in the final cycle for RB222 dye. The results showed that the synthesized $MgFe_2O_4$@$ZnAl_2O_4$ MNCs had excellent potential to be used as useful and efficient reusable photocatalyst.

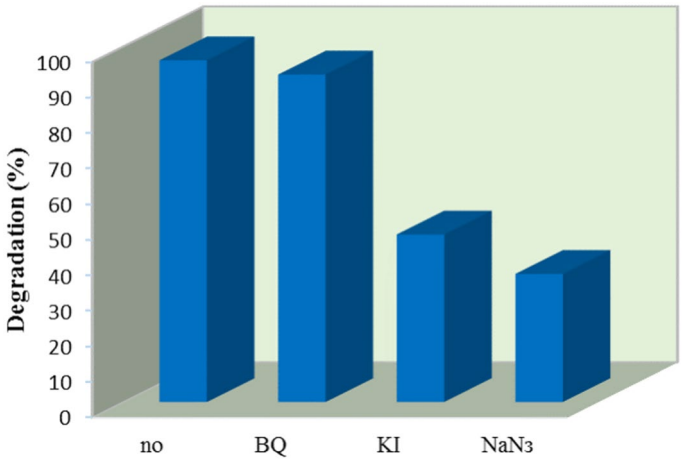

Figure 10. Impact of scavenging agents on RB222 dye degradation.

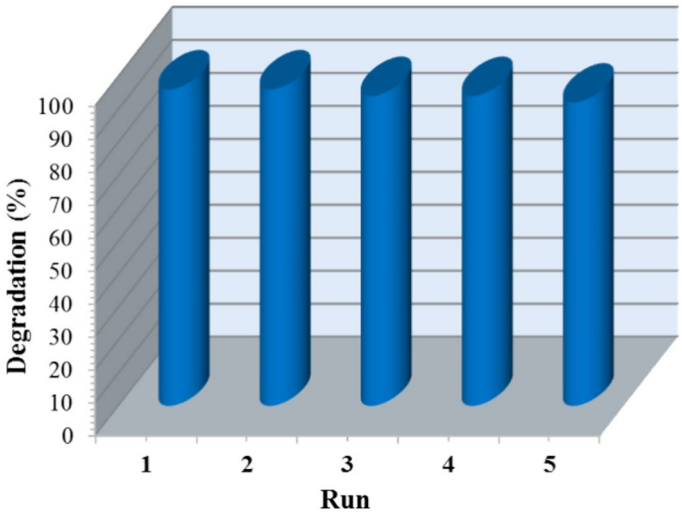

Figure 11. Recyclability of $MgFe_2O_4$@$ZnAl_2O_4$ MNCs. Reaction conditions: RB222 = 20 mg/l, catalyst = 0.02 g, 10 min.

Conclusions

In conclusion, $MgFe_2O_4$@$ZnAl_2O_4$ magnetic nanocomposites were successfully synthesized with the easy, green, and cost-effective sol–gel method. Base on the XRD pattern, magnetic nanocomposites were produced in very pure spinel structure within crystallite size 13 nm. Also, SEM and TEM images revealed that morphology of nanocomposites is spherical with average width of 20–25 nm. The nanocomposites exhibited a saturation magnetization (Ms) of 6.59 emu/g, confirming their superparamagnetic nature due to the absence of Hc and Mr values. BET analysis revealed a surface area of 78.109 m^2/g, while DRS analysis determined a band gap of 1.88 eV. Photocatalytic, photolysis, and adsorption performance evaluations demonstrated superior photodegradation activity, indicating a synergistic effect between $MgFe_2O_4$@$ZnAl_2O_4$ MNCs and visible light irradiation for organic dye degradation. Specifically, 96% degradation of RB222 dye was achieved within 10 min, with a corresponding TOC removal rate of around 59%. The $MgFe_2O_4$@$ZnAl_2O_4$ MNCs was used as useful photocatalyst for degradation of RB222 dye. Photocatalytic activity under the visible light irradiation, low catalyst dosage, high concentration of pollutants**,** short irradiation time, and reusability the nanocomposites are the merits of this work and shown these photocatalysis have the promising potential for wastewater treatment.

Data availability

The data that support the findings of this study are available from the corresponding author upon reasonable request.

Received: 14 March 2024; Accepted: 15 July 2024
Published online: 19 July 2024

References

1. Nazim, M., Khan, A. A. P., Asiri, A. M. & Kim, J. H. Exploring rapid photocatalytic degradation of organic pollutants with porous CuO nanosheets: Synthesis, dye removal, and kinetic studies at room temperature. *ACS Omega* **6**, 2601–2612 (2021).
2. Tkaczyk, A., Mitrowska, K. & Posyniak, A. Synthetic organic dyes as contaminants of the aquatic environment and their implications for ecosystems: A review. *Sci. Total Environ.* **717**, 137222 (2020).
3. Rad, T. S., Ansarian, Z., Khataee, A., Vahid, B. & Doustkhah, E. N-doped graphitic carbon as a nanoporous MOF-derived nanoarchitecture for the efficient sonocatalytic degradation process. *Sep. Purif. Technol.* **256**, 117811 (2021).
4. Moradnia, F., Taghavi Fardood, S., Ramazani, A., Osali, S. & Abdolmaleki, I. Green sol–gel synthesis of $CoMnCrO_4$ spinel nanoparticles and their photocatalytic application. *Micro Nano Lett.* **15**, 674–677. https://doi.org/10.1049/mnl.2020.0189 (2020).
5. Messaoudi, Z. A. *et al.* Adsorption and photocatalytic degradation of crystal violet dye under sunlight irradiation using natural and modified clays by zinc oxide. *Chem. Method.* **6**, 661–676. https://doi.org/10.22034/chemm.2022.340376.1507 (2022).
6. Moussavi, G. & Mahmoudi, M. Removal of azo and anthraquinone reactive dyes from industrial wastewaters using MgO nanoparticles. *J. Hazard. Mater.* **168**, 806–812 (2009).
7. Dil, E. A., Ghaedi, M., Asfaram, A., Mehrabi, F. & Bazrafshan, A. A. Optimization of process parameters for determination of trace Hazardous dyes from industrial wastewaters based on nanostructures materials under ultrasound energy. *Ultrason. Sonochem.* **40**, 238–248 (2018).
8. Ahmed, A. *et al.* Efficient photocatalytic degradation of toxic Alizarin yellow R dye from industrial wastewater using biosynthesized Fe nanoparticle and study of factors affecting the degradation rate. *J. Photochem. Photobiol. B.* **202**, 111682 (2020).
9. Sabouri, Z., Sammak, S., Sabouri, S., Tabrizi Hafez Moghaddas, S. S. & Darroudi, M. Green synthesis of Ag-Se doped ZnO–Co_3O_4–NiO fivenary nanocomposite using poly anionic cellulose and evaluation of their anticancer and photocatalyst applications. *Chem. Method.* **8**, 164–176. https://doi.org/10.48309/chemm.2024.436507.1758 (2024).
10. Ali, F., Fazal, S., Iqbal, N., Zia, A. & Ahmad, F. PANI-based nanocomposites for the removal of dye from wastewater. *J. Med. Nanomater. Chem.* **5**, 106–124. https://doi.org/10.48309/jmnc.2023.2.1 (2023).
11. Amar, I. A. *et al.* Photocatalytic degradation of malachite green dye under UV light irradiation using calcium-doped ceria nanoparticles. *J. Med. Nanomater. Chem.* **2**, 1–14. https://doi.org/10.48309/jmnc.2020.1.1 (2020).
12. Mehdizadeh, P., Orooji, Y., Amiri, O., Salavati-Niasari, M. & Moayedi, H. Green synthesis using cherry and orange juice and characterization of $TbFeO_3$ ceramic nanostructures and their application as photocatalysts under UV light for removal of organic dyes in water. *J. Clean. Prod.* **252**, 119765 (2020).
13. Anis, S. M. *et al.* Decorated ZrO_2 by Au nanoparticles as a potential nanocatalyst for the reduction of organic dyes in water. *Inorg. Chem. Commun.* **141**, 109489 (2022).
14. Ismail, M. *et al.* Green synthesis of plant supported CuAg and CuNi bimetallic nanoparticles in the reduction of nitrophenols and organic dyes for water treatment. *J. Mol. Liq.* **260**, 78–91 (2018).
15. Moradnia, F. *et al.* Green synthesis of nickel oxide nanoparticles using plant extracts: An overview of their antibacterial, catalytic, and photocatalytic efficiency in the degradation of organic pollutants. *Iran. J. Catal. (IJC)* **14**, 1–24. https://doi.org/10.57647/j.ijc.2024.1401.01 (2024).
16. Ahmed, A., Usman, M., Yu, B., Shen, Y. & Cong, H. Sustainable fabrication of hematite (α-Fe_2O_3) nanoparticles using biomolecules of *Punica granatum* seed extract for unconventional solar-light-driven photocatalytic remediation of organic dyes. *J. Mol. Liq.* **339**, 116729. https://doi.org/10.1016/j.molliq.2021.116729 (2021).
17. Bibi, F. *et al.* Fabrication of Ni and Mn co-doped $ZnFe_2O_4$ spinel ferrites and their nanocomposites with rGO as an efficient photocatalyst for the remediation of organic dyes. *Polyhedron* **250**, 116826. https://doi.org/10.1016/j.poly.2024.116826 (2024).
18. Moghaddas, S. M. T. H., Elahi, B. & Javanbakht, V. Biosynthesis of pure zinc oxide nanoparticles using Quince seed mucilage for photocatalytic dye degradation. *J. Alloys Compd.* **821**, 153519 (2020).
19. Nur, A. S. *et al.* A review on the development of elemental and codoped TiO_2 photocatalysts for enhanced dye degradation under UV–Vis irradiation. *J. Water Process Eng.* **47**, 102728 (2022).
20. Tomar, R., Abdala, A. A., Chaudhary, R. & Singh, N. Photocatalytic degradation of dyes by nanomaterials. *Mater. Today Proc.* **29**, 967–973 (2020).
21. Al-Mamun, M., Kader, S., Islam, M. & Khan, M. Photocatalytic activity improvement and application of UV–TiO_2 photocatalysis in textile wastewater treatment: A review. *J. Environ. Chem. Eng.* **7**, 103248 (2019).
22. Ge, M., Hu, Z., Wei, J., He, Q. & He, Z. Recent advances in persulfate-assisted TiO_2-based photocatalysis for wastewater treatment: Performances, mechanism and perspectives. *J. Alloys Compd.* **888**, 161625 (2021).
23. Elanthamilan, E., Elizabeth, I. B., Wang, S.-F. & Lydia, I. S. Strontium hexaferrite microspheres: Synthesis, characterization and visible-light-driven photocatalytic activity towards the degradation of methylene blue dye. *Opt. Mater.* **137**, 113565. https://doi.org/10.1016/j.optmat.2023.113565 (2023).

24. Ahmed, D. *et al.* Efficient degradation of atrazine from synthetic water through photocatalytic activity supported by titanium dioxide nanoparticles. *Z. Phys. Chem.* **237**, 395–412. https://doi.org/10.1515/zpch-2022-0123 (2023).
25. Zamani, A., Asghari, S. & Tajbakhsh, M. Synthesis of TiO_2/CD and TiO_2/Ag/CD nanocomposites and investigation of their visible light photocatalytic activities in the degradation of methylene blue. *Chem. Method.* **8**, 177–199. https://doi.org/10.48309/chemm.2024.432168.1753 (2024).
26. Kalia, S. *et al.* Magnetic polymer nanocomposites for environmental and biomedical applications. *Colloid. Polym. Sci.* **292**, 2025–2052 (2014).
27. Yi, D. K., Lee, S. S. & Ying, J. Y. Synthesis and applications of magnetic nanocomposite catalysts. *Chem. Mater.* **18**, 2459–2461 (2006).
28. Yang, Q. *et al.* Design of functional magnetic nanocomposites for bioseparation. *Colloids Surf. B. Biointerfaces* **191**, 111014 (2020).
29. Teja, A. S. & Koh, P.-Y. Synthesis, properties, and applications of magnetic iron oxide nanoparticles. *Prog. Cryst. Growth Charact. Mater.* **55**, 22–45 (2009).
30. Sharma, P., Dutta, D., Udayan, A. & Kumar, S. Industrial wastewater purification through metal pollution reduction employing microbes and magnetic nanocomposites. *J. Environ. Chem. Eng.* **9**, 106673 (2021).
31. Gupta, T. & Chauhan, R. P. Enhanced photocatalytic degradation of cationic dye using Cu-doped ZnSe. *Opt. Mater.* **135**, 113295. https://doi.org/10.1016/j.optmat.2022.113295 (2023).
32. Ahmed, A. *et al.* Facile synthesis of Zr^{4+} substituted $Mn_{0.2}Co_{0.8}Fe_{2-x}O_4$ nanoparticles and their composites with reduced graphene oxide for enhanced photocatalytic performance under visible light irradiation. *Synth. Met.* **277**, 116766. https://doi.org/10.1016/j.synthmet.2021.116766 (2021).
33. Moradnia, F., Taghavi Fardood, S. & Ramazani, A. Green synthesis and characterization of $NiFe_2O_4$@$ZnMn_2O_4$ magnetic nanocomposites: An efficient and reusable spinel nanocatalyst for the synthesis of tetrahydropyrimidine and polyhydroquinoline derivatives under microwave irradiation. *Appl. Organomet. Chem.* **38**, e7315. https://doi.org/10.1002/aoc.7315 (2023).
34. Noroozi Pesyan, N., Batmani, H. & Havasi, F. Copper supported on functionalized MCM-41 as a novel and a powerful heterogeneous nanocatalyst for the synthesis of benzothiazoles. *Polyhedron* **158**, 248–254. https://doi.org/10.1016/j.poly.2018.11.005 (2019).
35. Taghavi Fardood, S., Moradnia, F., Heidarzadeh, S. & Naghipour, A. Green synthesis, characterization, photocatalytic and antibacterial activities of copper oxide nanoparticles of copper oxide nanoparticles. *Nanochem. Res.* **8**, 134 (2023).
36. Tai, L. T. *et al.* Green synthesis of copper oxide nanoparticles for photodegradation of malachite green and antibacterial properties under visible light. *Opt. Mater.* **136**, 113489. https://doi.org/10.1016/j.optmat.2023.113489 (2023).
37. Ali, A. *et al.* Synthesis of visible light responsive $Ce_{0.2}Co_{0.8}Fe_2O_4$/g-C_3N_4 composites for efficient photocatalytic degradation of rhodamine B. *Diamond Relat. Mater.* **133**, 109721. https://doi.org/10.1016/j.diamond.2023.109721 (2023).
38. Ahmed, A. *et al.* Synthesis of visible-light-responsive lanthanum-doped copper ferrite/graphitic carbon nitride composites for the photocatalytic degradation of toxic organic pollutants. *Diamond Relat. Mater.* **141**, 110630. https://doi.org/10.1016/j.diamond.2023.110630 (2024).
39. Taghavi Fardood, S. *et al.* Green synthesis and characterization of α-Mn_2O_3 nanoparticles for antibacterial activity and efficient visible-light photocatalysis. *Sci. Rep.* **14**, 6755. https://doi.org/10.1038/s41598-024-56666-2 (2024).
40. Ahankar, H., Taghavi Fardood, S. & Ramazani, A. One-pot three-component synthesis of tetrahydrobenzo [b] pyrans in the presence $Ni_{0.5}Cu_{0.5}Fe_2O_4$ of magnetic nanoparticles under microwave irradiation in solvent-free conditions. *Iran. J. Catal.* **10**, 195–201 (2020).
41. Taghavi Fardood, S. *et al.* Green synthesis of ZnO nanoparticles via sol-gel method and investigation of its application in solvent-free synthesis of 12-aryl-tetrahydrobenzo[α]xanthene-11-one derivatives under microwave irradiation. *Chem. Method.* **3**, 632–642. https://doi.org/10.33945/sami/chemm.2019.6.2 (2019).
42. Su, N. R. *et al.* Fabrication of $MgFe_2O_4$–ZnO heterojunction photocatalysts for application of organic pollutants. *Mater. Lett.* **122**, 201–204 (2014).
43. Makofane, A. *et al.* Green synthesis of $NiFe_2O_4$ nanoparticles for the degradation of methylene blue, sulfisoxazole and bacterial strains. *Inorg. Chem. Commun.* **139**, 109348 (2022).
44. Jia, J., Du, X., Zhang, Q., Liu, E. & Fan, J. Z-scheme $MgFe_2O_4$/Bi_2MoO_6 heterojunction photocatalyst with enhanced visible light photocatalytic activity for malachite green removal. *Appl. Surf. Sci.* **492**, 527–539. https://doi.org/10.1016/j.apsusc.2019.06.258 (2019).
45. Moradnia, F., Taghavi Fardood, S., Ramazani, A. & Gupta, V. K. Green synthesis of recyclable $MgFeCrO_4$ spinel nanoparticles for rapid photodegradation of direct black 122 dye. *J. Photochem. Photobiol. A.* **392**, 112433 (2020).
46. Taghavi Fardood, S. *et al.* Biosynthesis of $MgFe_2O_4$ magnetic nanoparticles and its application in photo-degradation of malachite green dye and kinetic study. *Nanochem. Res.* **4**, 86–93 (2019).
47. Kiani, M. T., Ramazani, A. & Taghavi Fardood, S. Green synthesis and characterization of $Ni_{0.25}Zn_{0.75}Fe_2O_4$ magnetic nanoparticles and study of their photocatalytic activity in the degradation of aniline. *Appl. Organomet. Chem.* **37**, e7053. https://doi.org/10.1002/aoc.7053 (2023).
48. Sing, K. S. Reporting physisorption data for gas/solid systems with special reference to the determination of surface area and porosity (provisional). *Pure Appl. Chem.* **54**, 2201–2218 (1982).
49. Taghavi Fardood, S., Yekke Zare, F., Moradnia, F. & Ramazani, A. Preparation, characterization and photocatalysis performances of superparamagnetic $MgFe_2O_4$@CeO_2 nanocomposites: Synthesized via an easy and green sol–gel method. *J. Rare Earths.* https://doi.org/10.1016/j.jre.2024.03.006 (2024).
50. Kamzin, A. S., Das, H., Wakiya, N. & Valiullin, A. A. Magnetic core/shell nanocomposites $MgFe_2O_4$/SiO_2 for biomedical application: Synthesis and properties. *Phys. Solid State* **60**, 1752–1761 (2018).
51. Moradnia, F. *et al.* Magnetic $Mg_{0.5}Zn_{0.5}FeMnO_4$ nanoparticles: green sol-gel synthesis, characterization, and photocatalytic applications. *J. Clean. Prod.* **288**, 125632 (2021).
52. Rafiq, A. *et al.* Photocatalytic degradation of dyes using semiconductor photocatalysts to clean industrial water pollution. *J. Ind. Eng. Chem.* **97**, 111–128 (2021).
53. Taghavi Fardood, S. *et al.* Facile green synthesis, characterization and visible light photocatalytic activity of $MgFe_2O_4$@ $CoCr_2O_4$ magnetic nanocomposite. *J. Photochem. Photobiol. A.* **423**, 113621 (2022).
54. Ali, F. *et al.* Recyclable Cu–Ag bimetallic nanocatalyst for radical scavenging, dyes removal and antimicrobial applications. *Chemosphere* **313**, 137321 (2023).
55. Kaeosamut, N. *et al.* synergistic induction of solvent and ligand-substitution in single-crystal to single-crystal transformations toward a MOF with photocatalytic dye degradation. *Inorg. Chem.* **62**, 19908–19921 (2023).
56. Akhtar, N. *et al.* Solar light-driven photocatalytic degradation potential of g-C_3N_4 based binary chalcogenides ($AgBiS_2$/g-C_3N_4). *Mater. Chem. Phys.* **316**, 129067. https://doi.org/10.1016/j.matchemphys.2024.129067 (2024).

Author contributions

S.T.F.: Supervision, Validation, Project administration, Conceptualization, Investigation, Methodology, Manuscript preparation and revision; S.G.: Investigation, Implementation of experiments, Methodology; F.M.: Investigation, Implementation of experiments, Methodology, and Manuscript preparation and revision; A.R.: Validation, discussion, Writing and review.

Competing interests
The authors declare no competing interests.

Additional information
Correspondence and requests for materials should be addressed to S.T.F.

Reprints and permissions information is available at www.nature.com/reprints.

Publisher's note Springer Nature remains neutral with regard to jurisdictional claims in published maps and institutional affiliations.